LANDSLIDE HAZARD MAPPING

PART 3: Prediction and Mapping of Landslide Hazard

By

Tien H. Wu and Mohamed Abdel-Latif

TIMBER/FISH
&WILDLIFE

December 1996
Revised June 1997

LANDSLIDE HAZARD MAPPING

PART 3: Prediction and Mapping of Landslide Hazard

By

Tien H. Wu and Mohamed Abdel-Latif

ACKNOWLEDGEMENTS

The work reported here was performed with financial support from the CMER Committee of the Washington Timber/Fish/Wildlife Agreement, and NASA's Center for Commercial Development of Space at Ohio State University. The writers are grateful to M.J. Brunengo, Washington Dept. of Natural Resources, who provided us with the statistics on rainfall and snow depth and the geological information derived from his field work in Glenoma and Mineral quadrangles. We also wish to thank members of the SHAMW Technical Steering Committee of Timber/Fish/Wildlife Agreement for their input to this study.

ABSTRACT

The report outlines a mechanics-based methodology for prediction and mapping of landslide hazard for hillside slopes. The principal components are: estimation of rain and snowmelt, estimation of infiltration and groundwater response, and estimation of failure probability.

Brunengo's (1989) statistical data on rainstorms and snow-on-ground were used to predict the rainfall-plus-snowmelt, which constitutes the infiltration at the ground surface. The lumped-parameter groundwater model of Reddi and Wu (1991) was used to predict overall infiltration and drainage from catchments. The finite-difference solution (Lee, 1986) was used to estimate the variations of groundwater levels within catchments. The infinite-slope model was used to predict slope failure and hazard. Predictions with the models are made by using the best estimates of the input parameters and the associated uncertainties. This allows us to account for different levels of accuracy in the available information and judgment based on field observations.

The method allows mapping of landslide hazard at different scales and with various degrees of refinement. In this project, mapping was done at two different levels: a macro-map made with regional site conditions and simplified groundwater profile, and a micro map made with local site conditions and a groundwater profile that accounts for catchment shape. Macro- and micro-hazard maps were produced for Glenoma and Mineral quadrangles.

TABLE OF CONTENTS -

LIST OF TABLES

LIST OF FIGURES

1. INTRODUCTION

1.1. PROBLEM STATEMENT

Landslides constitute one of the major natural hazards, causing loss of lives and property and degradation of environment. In the lower and middle elevations of mountains in Washington, landslides occur frequently following intense rain and especially rain-on-snow events, when rain plus snowmelt infiltrate into the soil (Berris and Harr, 1987). Snow accumulation prior to and snowmelt during such events are believed to be influenced by vegetation on the slopes. Since logging significantly changes the vegetative cover, it is expected to affect snow accumulation and snowmelt and occurrence of landslides. Accordingly, landslide hazard should be considered in the management of forested watersheds. Because future events cannot be predicted with certainty, management decisions are made under conditions of uncertainty. In probabilistic decision theory, the decision process should account for the hazard and risk of landslides and the utilities of the management options. Hence, landslide hazard prediction and mapping is a requirement in decision making.

The mechanics of storm-induced landslides includes the following components (Fig. 1a). During a rain-on-snow event, rain plus snowmelt constitute the source for infiltration into the soil. A part of the water that infiltrates into the soil reaches the saturated zone as recharge, and causes a rise in the piezometric level, h_w. The saturated zone is drained by gravity flow which reduces h_w (Fig. 1b). Hence, the change in h_w is the recharge minus the drainage. A rise in h_w reduces the shear strength and increases the seepage force in the soil. The net result is a reduction in the safety factor (F_s) with respect to slope failure. These three components are called rain-on-snow, slope hydrology, and slope stability, respectively. Development of models to predict the response of the three components is required for prediction of landslide hazard.

This project is a continuation of its predecessor, *Landslide Hazard Mapping. Part 1, Estimation of Piezometric Levels*. In this project, the results from Part 1 were used to construct landslide

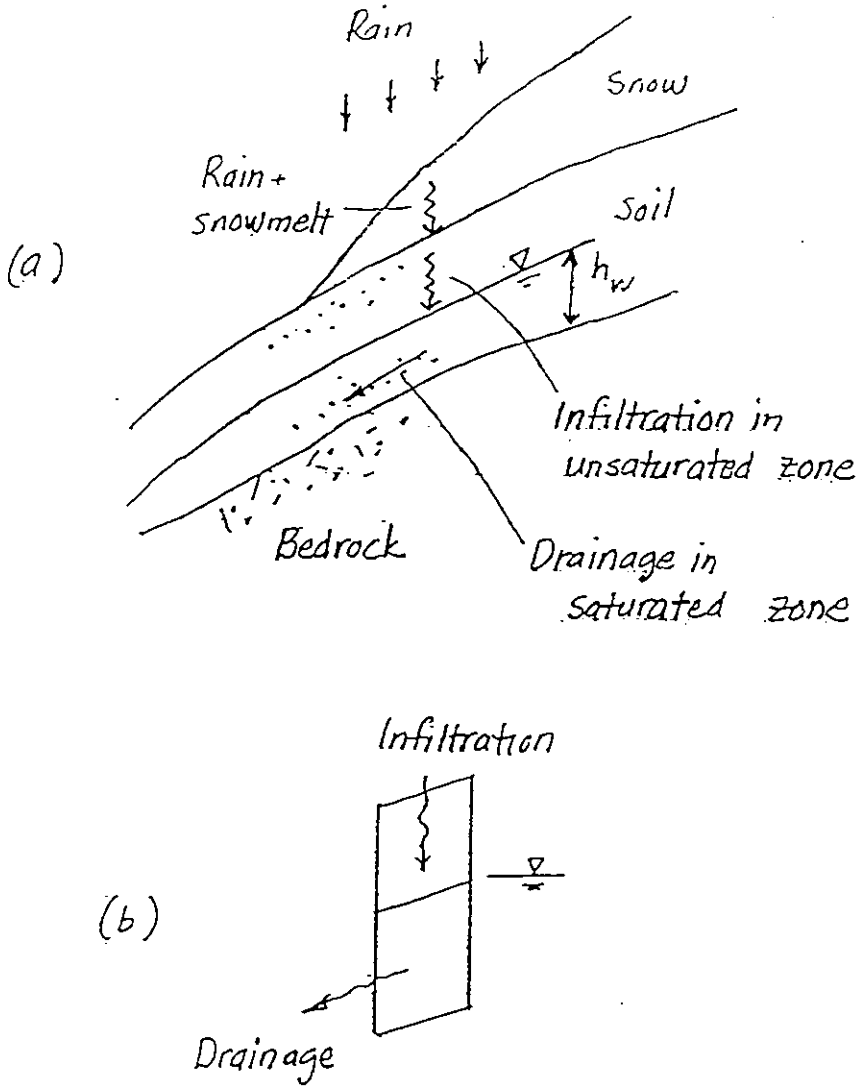

Figure 1. Components of (a) landslide hazard assessment system (b) groundwater flow.

hazard maps for Glenoma and Mineral quadrangles. To provide a complete and self-contained report, we present here the procedures used in the entire project for the construction of landslide hazard maps. Details on estimating piezometric levels that are considered to be of minor importance are not repeated here. The reader is referred to the report on Part 1 (Wu et al.,1993) for these details.

1.2. OBJECTIVE AND SCOPE

The objective of this research is to develop the methodology for prediction and mapping of landslide hazard in the lower and middle elevations of the Cascade Mountains of Washington. The results are intended for use by land managers and foresters for evaluation of slope stability after logging. Landslide hazard maps may be used in level 1 of Washington's watershed analysis process, and the results of watershed analysis may be used for updating the landslide hazard maps. Because of the nature of the information used in the prediction, the predicted hazards are considered as preliminary estimates. Such hazard maps can be produced at minimal cost prior to detailed field investigations, and can be used for preliminary planning of land use and for planning of more detailed investigations.

1.3. LITERATURE REVIEW

A variety of landslide hazard maps have been constructed, usually from detailed field data. A brief list of examples include maps constructed from landslide inventories (Brabb et al., 1972; Wieczorek, 1984), by consideration of site conditions including lithology, rock structure, hydrology, and their relation to topography (Wagner et al., 1987), or by statistical correlation of landslide frequency with geologic and geomorphic factors (Carrara et al., 1991). Because of the large areal coverage, material properties from detailed site investigations are usually not available for mapping.

In the terminology proposed by Einstein (1988), "hazard maps" indicate failure probabilities in different areas of a region. Typically, failure in shallow soils on hillside slopes during or after rainstorms is induced by an increase in porepressure and a corresponding reduction in effective stress in the soil (Terzaghi, 1950). This mechanism has been analyzed by combining a hydrologic

model with a slope stability model (Fell, 1991, Sammori and Tsuboyama, 1991). Estimation of failure probability based on infiltration of rainfall and soil strength have been made by Ward et al. (1978), Wu and Swanston (1980), Hammond et al. (1991).

2. METHODS AND RESULTS

The prediction methodology described in this paper extends the earlier works by systematically accounting for all the known uncertainties in the input variables for the models, and translating these into a failure probability. The first two components of the landslide hazard prediction methodology are prediction of rainfall and snowmelt, and prediction of groundwater response via infiltration and drainage; the third component is stability analysis and evaluation of failure probability; the fourth component is mapping. This methodology was used to construct a landslide hazard map for Glenoma and Mineral quadrangles, WA., using published data on storm characteristics, soil properties from soil survey reports, and topographic data from the U.S. Geological Survey. The input for prediction consists of the mean values of the pertinent parameters, which reflect the best estimates, and the variances, which represent the uncertainties. A set of best estimates and uncertainties is associated with each set of input parameters.

2.1. STORM MODEL

The area of concern lies in the transient snow zone in the Cascade Mountains of Washington. The transient snow zone is an area where snow typically accumulates and melts several times during a winter. When significant amounts of rain fall on ripe snow packs, large amounts of water can infiltrate into hillside slopes during a few days (Berris and Harr,1987), causing floods and landslides. A storm model is used to generate the rainfall (R) and snowmelt (M) which constitute the water available for infiltration,

$$I = M + R \qquad [1]$$

If there is no snow on the ground, then M = 0. The probability density function (pdf) of I is

$$f(I) = f(I=R|\ S=0)P(S=0) + f(I=M+R|\ S>0)P(S>0) \qquad [2]$$

where f(.)=pdf, p(.)= probability, f (x|y) = conditional pdf of x given y, S = snow depth, in terms of snow-water equivalent. The storm characteristics needed for modeling rain-on-snow events are snow depth and rainfall characteristics. Data on snow depths (Brunengo,1989) and "long continuous storms" (LCS), defined as storms bounded by periods of 6 hrs. or more with no rainfall (Brunengo, 1989), were used to derive the mean and variance for I per storm (Wu et al., 1995). LCS were used here because they can provide enough rainfall and snowmelt to initiate slope failures.

For a design life of m years, the worst case is the maximum I during that period, or the maximum value of I from m samples (I_m). The pdf of I_m and its mean and variance are derived in Appendix A for m=10 years. Studies by Bras and Rodriguez-Iturbe (1985) indicate spatial correlation in rainfall intensity up to several kilometers. Hence, variations in rainfall within a catchment is ignored.

2.2. SITE CONDITIONS

The site condition is derived from published information, which consists of USGS topographic maps and county soil survey reports (Soil Conservation Service, 1987). The slopes are determined from the topographic maps. The "general soil map" and the "detailed soil map" in soil survey reports give the areal distribution of soil associations and soil series phases, respectively. The properties associated with each soil association and each soil series phase are ranges in soil depth, H, and saturated permeability, K_S. From these, we derived the mean soil depth and the geometric mean of the permeability. Other soil properties that are needed for calculations are: ψ_S and B, the parameters for unsaturated permeability, K (θ), and suction, ψ (θ), which are written as (Campbell, 1974; Beven, 1982)

$$K(\theta) = K_s(\theta/\theta_s)^{2B+3} \qquad [3]$$

$$\psi(\theta) = \psi_s (\theta/\theta_s)^{-B} \qquad [4]$$

and θ_d and θ_s, the drainable and saturated volumetric moisture content. These properties are usually not available in soil survey reports. For the present case, these properties were estimated from the data of Clapp and Hornberger (1978) and test results from similar soils (Hammond et al.,1991; Schroeder, 1983). The properties for soil associations are applicable to Glenoma and Mineral quadrangles and are called regional properties. These are summarized in Table 1.2a and b, Col.2 and 3. Properties for soil-series phases are called local properties. A catchment usually contains two or more soil-series phases. An example of local properties is given in Table 1, Col. 5 and 6. The values of x_1 and x_2 denote mean permeabilities of two soil-series phases in Catchment 77. These properties represent the best information available in the absence of a specific site investigation.

Uncertainties about the site conditions include inaccuracies in topographic data and uncertainties about soil properties. The errors in slope due to inaccuracies in topographic data are small (Abdel-Latif,1994) and are ignored. Uncertainties about soil properties arise because of systematic errors and spatial variations. In addition, it is common to observe geologic features, herein called anomalies because they are not described in published reports. These values are used to obtain a mean (μ), a standard deviation (σ), or variance = Var [.] = σ^2 , and a coefficient of variation = COV =Δ = σ/μ.. The mean represents the best estimate, while the other three represent the uncertainty. The uncertainties associated with the various sources or error are described below.

SYSTEMATIC ERRORS. Systematic errors are present because the soil properties given in soil survey reports may be in error due to the small number of samples and the judgement and extrapolation used to arrive at the values. Systematic errors are also introduced when soil properties are taken from publications because the soil may be different from that at the site, even though the descriptions are similar. The systematic error is expressed as a coefficient of variation

Table 1. Site Conditions

(a) Soil Properties - Infiltration and Drainage Model

	Glenoma and Mineral Quadrangles			Catchment #77							
(1)	(2)	(3)	(4)	(5)	(6)	(7)	(8)	(9)	(10)	(11)	(12)
Parameter	Range	Mean		x_1	x_2	X_A	Δ_x	δ(m)	Γ	Var[X_A]	Δ_A
K_S	0.5 -15 (cm/hr)	2.8	0.82	6.0	2.0	3.1	1.1	1.5	0	7.9	1.03
H	0.5 - 1.5 (m)	1	0.29	1.5	0.75	1.0	0.23	1	0	0.17	0.42
θ_d	0.29 - 0.35	0.32	0.06	0.32	0.32	0.32	.36	1.5	0	.0003	0.06
θ_S	0.6 - 0.5	0.45	0.05	0.45	0.45	0.45	-	-	0	.0005	0.05
β	4.0 - 5.0	4.38	0.34	4.38	4.38	4.38	-	-	0	2.16	0.34
ψ_S	7.0 - 30 (cm)	10.0	1.22	10.0	10.0	10.0	-	-	0	150	1.22

(b) Soil Properties - Stability Model

	Glenoma and Mineral Quadrangles			Pixel in Catchment #77							
(1)	(2)	(3)	(4)	(5)	(6)	(7)	(8)	(9)	(10)	(11)	(12)
ϕ'	25 - 35°	30	0.10	32	-		0.45	3.0	0.30	1.1	0.34
c'	1.67 - 4.54 (kPa)	3.11	0.30	3.51	-		.11	3.0	0.30	9.7	0.11
H	0.5 - 1.5 (m)	1	0.29	1.0	-		0.23	1	0.18	0.081	0.29

(COV), Δ_S, of the mean, as given in Tables 1a and b, Col. 4. The COV is taken to be that of a uniform distribution between the range given in Col.2.

SPATIAL VARIATIONS. Spatial variations in soil properties also cause uncertainties about the mean value. Fig.2a illustrates a hypothetical section that cuts through several soil types, with the soil property X plotted on the vertical axis. The dashed line and x_i represent the mean values of X for soil i; these are subject to systematic uncertainty. Values of x_1 and x_2 for Catchment 77 are given in Table 1a, Cols. 5 and 6. The subscripts 1 and 2 refer to two different soil-series phases found within the catchment. Spatial variations are caused by the changes in soil type (i), leading to occurrence uncertainty, and by random variations within each soil type shown by the solid curve in Fig.2a. The occurrence uncertainty reflects uncertainty about the type of material present at a given point, and is expressed in terms of the ratio a_j/a_i, where a_i and a_j = the mean dimensions of materials i and j. This ratio is a random variable because a_i and a_j are not known with certainty. The variance of the average of the property X over region A (X_A) due to the combined systematic and occurrence uncertainties is (Tang and Gilbert, 1988).

$$\text{Var}[X_A] = \mu_{x1}^2 [(1-\mu_\lambda)^2 \Delta_{S,1}^2 + (\mu_\lambda)^2 \Delta_{S,2}^2 \xi^2 + (1-\xi)^2 \text{Var}[\lambda_A] \quad [5]$$

where $\lambda = 1/[1 + (a_2/a_1)]$, $\xi = x_2/x_1$, μ_λ = mean of λ, μ_{xi} = mean of x_i. Expressions for μ_λ and Var [λ_A] are given in Tang and Gilbert (1988).

Random variations within a soil type are expressed as a COV, Δ_r, of the point data and a correlation distance, δ, that represents "the distance within which the soil properties show relatively strong correlation" (Vanmarcke,1977). Examples of large and small correlation distances are given in Fig. 2b and c. The uncertainty about the average X_A over a_i due to random variations decreases as a_i increases relative to δ. The relationship can be expressed as a COV,

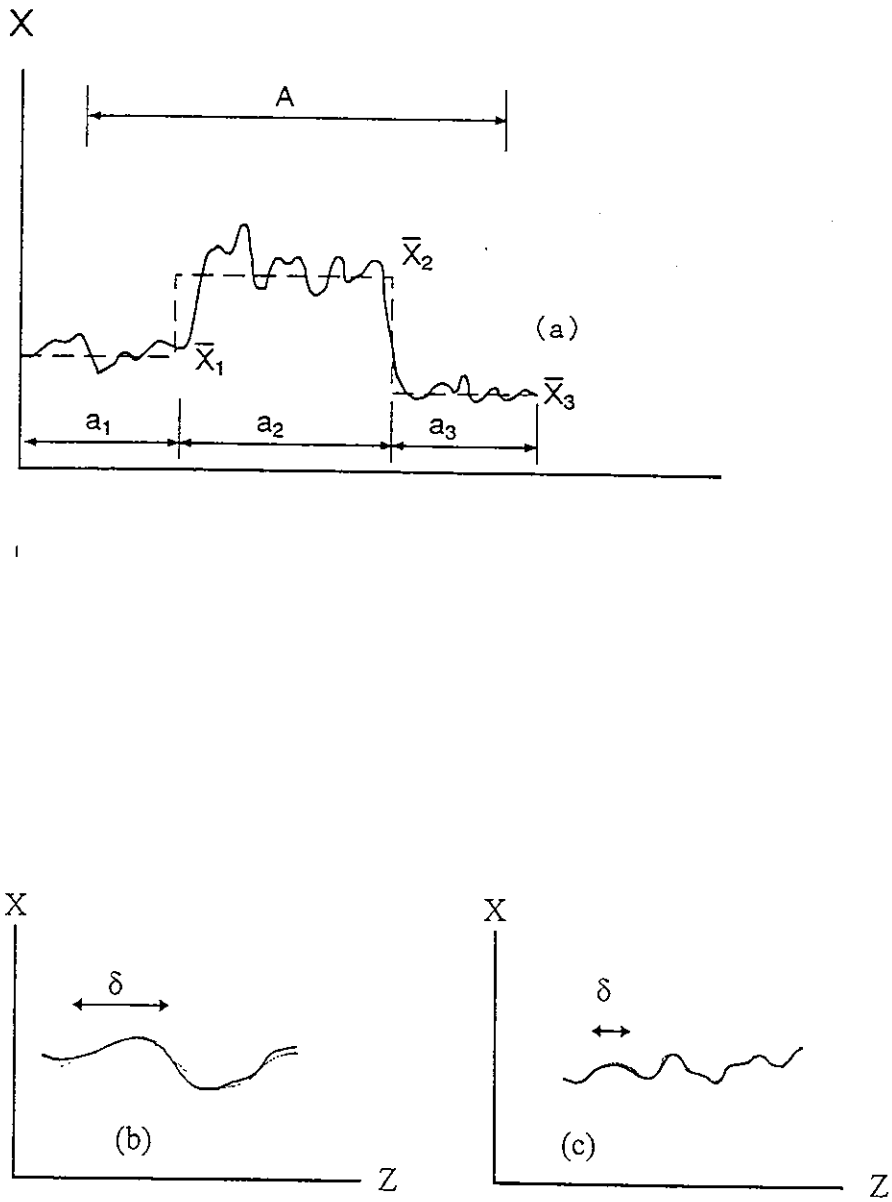

Fig. 2. Fig. 2. Spatial Variations. (a) Occurrence and random uncertainties, (b) Random variations with large δ, (c) Random variations with small δ

$$\Delta_{i,r}^2 = \Gamma^2(a_i)\ \Delta_r^2 \qquad [6]$$

where $\Gamma(a_i)$ = the variance function that depends on δ and a_i ; for a given δ, $\Gamma(a_i)$ decreases exponentially from 1, for very small a_i's, and approaches 0 at very large a_i's (Vanmarcke,1977). The parameters Δ_r and δ, which reflect random variations, are estimated from published data (Lumb, 1970; Tang, 1984; Wu, 1989), and given in Cols. 8 and 9 Table 1.

In general, all three sources of uncertainty are present. For the average over a catchment, the uncertainty due to random variations is small because δ is small compared to a_i and $\Gamma(a_i) = 0$ in Eq.[6]. The uncertainty about average properties for drainage and infiltration in a catchment (Cols. 11 and 12 in Table 1a) consists only of systematic and occurrence uncertainties and was calculated with Eq. [5]. For the average over a pixel, which is 30 x 30m, the occurrence uncertainty is zero because it is assumed that the soil type is known from the detailed soil map. Then we have only systematic uncertainty and uncertainty due to random variations. These are assumed to be independent, so the COV that represents the uncertainty about the average over area A is

$$\Delta_A^2 = \Delta_s^2 + \Delta_r^2 \qquad [7]$$

Eq [7] was used to calculate the uncertainties about the pixel average (Cols.11 and 12 in Table 1b).

GEOLOGIC ANOMALIES. For infiltration and drainage, the most important geologic anomalies are those that lead to flow through macropores (eg. Beven and Germann, 1982). Macropores identified by field observations in Glenoma and Mineral quadrangles include fractures in the bedrock and pervious inclusions in the soil layer. Because of the limited extent of the observations, the presence of such features is not known with certainty. Observations on these anomalies are described below.

Pervious inclusions in the soil layer serve as zones of high seepage velocity. In Glenoma and Mineral quadrangles the most important type of pervious inclusion is a pumice layer composed of particles of 1-2 cm. in diameter. The layer may be from 5 to 30 cm in thickness and is widespread. A hypothetical profile and cross-section is shown in Fig. 3. A pumice layer may be broken or interrupted, as shown in Fig. 3a. However, the width of the break in the Y direction is expected to be less than 2 m. The pumice is assumed to be present wherever pumice is mentioned in the description of a soil series, although the profiles do not show a distinct pumice layer.

Fractures in bedrock provide avenues of seepage. A simplified model of interconnected fractures is shown in Fig.4. The controlling parameter is the length of interconnected fractures. The extrapolation of limited observations onto the entire region of interest also involves uncertainties. In the absence of extensive data, subjective probabilities based on observations are used. The assumed probability distributions of the dimensions a_f and b_f in Fig. 4 are given in Table 2. The probability of the presence of fractures was assumed to be 1.0 everywhere.

Table 2 Distribution of Parameters for Fractured Rock

Variable	Distribution	Range	Mean	Variance	Sensitivity
K_f/K_s	lognormal	0.1-100	3.0	23.2	0.033
a_f/B_f	uniform	0.1-0.67	0.33	0.037	-0.056
b_f/L	lognormal	0.01-0.9	0.1	$5.6*10^{-3}$	1.51

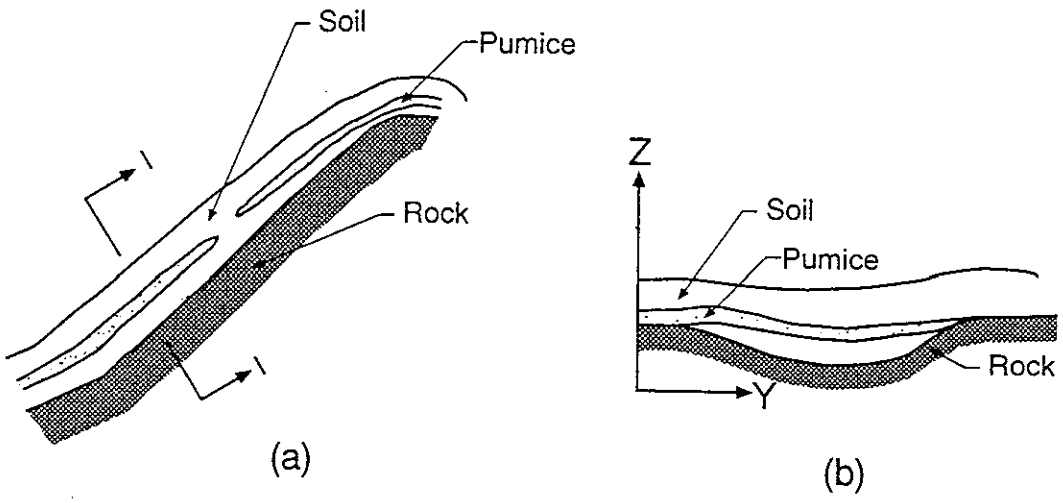

Fig. 3. Pumice layer, (a) Profile upslope, (b) Section 1-1

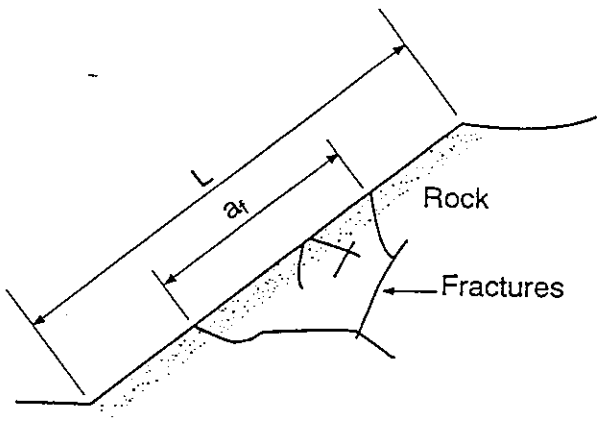

Fig. 4. Upslope profile of fractures in bedrock; b_f = width of ractures perpendicular to profile.

2.3. INFILTRATION AND DRAINAGE

Several methods are available for solving the infiltration in the unsaturated zone and the drainage in the saturated zone. The most sophisticated is to solve the three-dimensional flow by numerical methods (eg. Freeze, 1971). Simplfied, lumped parameter models have been proposed by Beven (1981, 1982), O'Loughlin (1988), Sloan and Moore (1984), Buchanan et al. (1990), and others.

Our method uses the lumped-parameter model to calculate the average water level in a catchment and a finite difference solution (Lee, 1986) to calculate the water level at different points within a catchment. The lumped-parameter model is shown in Fig.5, with average slope (α), convergence angle (ß), and soil thickness (H). The unsaturated zone above the phreatic surface is separated into three zones, as described in Eagleson (1978). Moisture movement between the three zones is computed by finite difference solution of the Richards equation (1931). The kinematic storage model of Beven (1981) is used for drainage in the saturated zone. Details of the model are given in Reddi and Wu (1991). The rainfall-plus-snowmelt (I) is applied at the ground surface and the model computes the water level h_0 at the exit point (Fig.5a) The peak value of h_0 for a given storm is used as an indicator of the groundwater level in a slope. For brevity, all subsequent references to h_0 imply the peak value.

For landslide hazard prediction, the mean of the maximum infiltration for the design period (Table 3a, Col. 2) and the mean soil properties for a catchment (Table 1a, Col 7) are used in the lumped-parameter model to predict the mean value of h_0. Where pumice is present the permeability is changed. The influence of small breaks in the continuity of the pumice on the flow is ignored. With a continuous pervious layer, the permeability for flow parallel to the slope is

$$K_p = [K_i H_i + K_s (H-H_i)]/H \qquad [8]$$

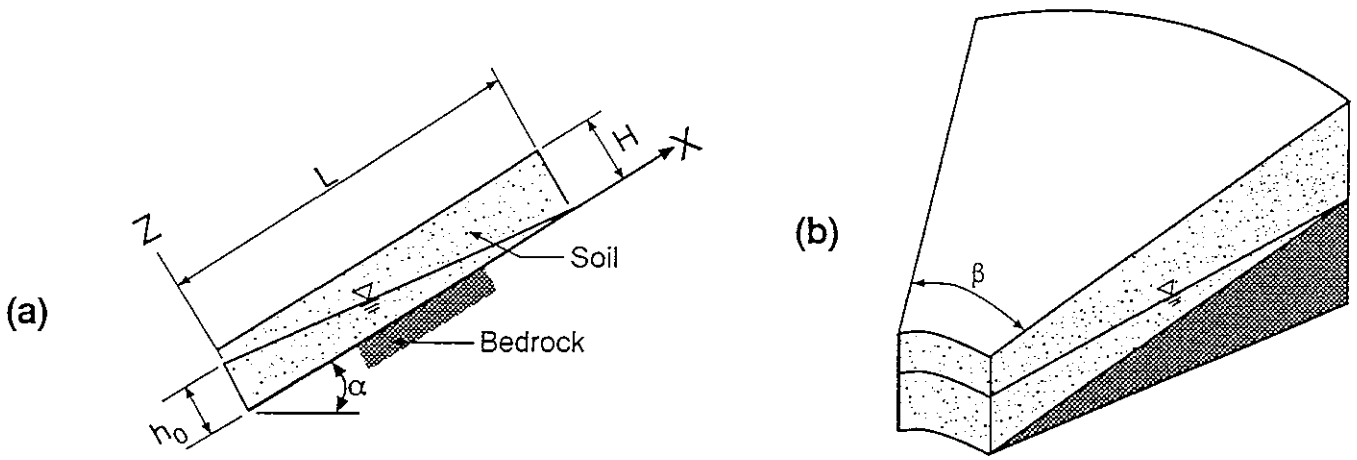

Fig. 5. Lumped parameter for infiltration and drainage, (Reddi and Wu, 1991)

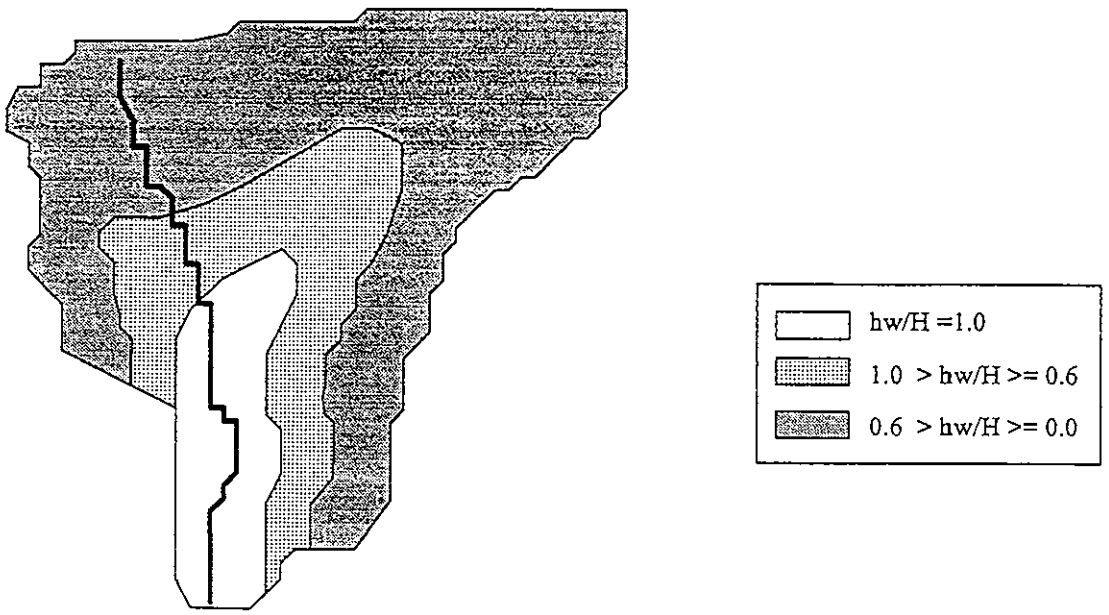

Fig. 6. Groundwater levels, h_w, calculated by finite difference solution, Catchment 77

where K_i and H_i = permeability and thickness, respectively, of the pervious inclusion. K_i is assumed to be $3.6x10^2$ m/hr, which is a typical value for gravel .The initial condition consists of the antecedent moisture condition: the mean of the initial moisture content, θ^0, and the mean of the initial water level, $h_0{}^0$. Calculations of θ^0 and $h_0{}^0$ for a sequence of storms are described in Appendix B. The values depend on the number of storms per season and the time interval between storms. The means and variances of θ^0 and $h_0{}^0$ for Glenoma Quadrangle are given in Table 3a, Cols. 2 and 3.

The water levels, h_W, at points within a catchment are calculated with the 2-dimensional finite difference solution which considers the non-planar surface of the catchment (Appendix C). An example is given in Fig. 6, which shows three zones of h_w for Catchment 77. The value of h_W/H is highest along the centerline of a converging slope (X-axis), which corresponds to the valley floor of a catchment. In this area, h_W/H is close to the value of h_0/H calculated by the lumped-parameter model. The value of h_W for each pixel within a catchment can be estimated by

$$h_w = \zeta h_0 \qquad [9]$$

Values of ζ are given in Appendix C. The soil properties are the same as those used in the lumped-parameter model.

Table 3. Uncertainties about Groundwater Levels

Random variable	Variable		Sensitivity	Var (ho)	C.O.V. (ho)
	Mean	Var			
(1)	(2)	(3)	(4)	(5)	(6)
(a) Storm uncertainty					
I_{10}	29.0 cm	51.2 cm^2	$2 * 10^{-2}$	0.021	0.22
θ^{o}	0.27	0.0025	2.68	0.003	0.084
$h_o{}^{o}/H$	0.38	0.31	0.64		
(b) Soil properties, systematic and occurrence uncertainties, catchment #77					
Ks	3.1 cm/hr	7.9	0.26	0.060	0.38
H	1 m	0.17	-0.44		
θ_d	0.32	0.0003	-0.82		
θs	0.45	0.0005	-1.60		
β	4.38	2.16	-0.05		
ψ_s	10.00	150	-0.0006		
(d) Fractures in bedrock					
K_f/K_s	3	2.3	0.0334	0.039	0.30
b/L	0.1	0.0056	1.508		
(e) Total				0.123	0.54

UNCERTAINTIES. The uncertainty about h_0/H can be estimated using the first-order second-moment (FOSM) method (Ang and Tang,1975), in which h_0/H is a function, g, of the random variables

$$h_0 / H = g [X_1, X_2, \ldots X_n] \qquad [10a]$$

where X_i = random variables, which are infiltration (I), antecedent moisture (θ^0 , $h_0{}^0$) , and soil properties. The variance of h_0 / H is

$$\text{Var} [h_0/H] = \Sigma \text{ Var} [X_i] \{d(h_0/H)/d X_i\}^2 \qquad [10b]$$

where d( ) denotes differential. The lumped-parameter model is used to evaluate $d(h_0/H)/ dX_i$, the sensitivity of h_0/H to uncertainties about I, θ^0, and $h_0{}^0$ (Table 3 Col.3), and to systematic and occurrence errors in soil properties (Table 1a, Col. 10,11). The variance of h_0/H is computed with Eq.[10]. The sensitivities to I, θ^0 , and $h_0{}^0$ and the corresponding variances of h_0/H for Glenoma Quadrangle are given in Table 3a. The sensitivities, and the corresponding variances of h_0/H for Catchment 77 are given in Table 3b. Calculations by Abdel-Latif (1994) show that, within the range in Table 1, the relation in Eq. [10 a] is approximately linear, so that FOSM may be used as an approximation.

Random variations in K_S and H cause local variations in h_W at the pixel level. Calculations by Lee (1988) and Abdel-Latif (1994) show that the COV due to random variations is small compared to those due to storm characteristics and systematic and occurrence uncertainties described in the preceding paragraph. Hence random variations are not considered here.

Transmissibility of a fracture can be estimated by several methods. Values of equivalent permeability for fractured rock reported by Huitt (1956) and Hoek (1981) range between 10^{-2} cm/sec. for joints filled with clay, to 10^{2} cm/sec. for heavily fractured rock. The equivalent permeability can also be expressed as (Louis, 1967)

$$K_f = g\, e^3 / 12\, \eta\, s \quad [11]$$

where g=gravitational acceleration, e=opening of fracture, b= joint spacing, and η = kinematic viscosity. For a spacing of 1 fracture/meter and e between 0.1 to 1 mm, the calculated K_f ranges from 10^{-4} to 10^{-1} cm/sec. The lower limit of these values is less than K_s, while the upper limit is about 100 times larger. Without actual measurement of the transmisibility, we assumed that the range of K_f/K_s may be from 0.1-100.

The 2-dimensional finite difference solution was also used to estimate the effect of flow through joints. The formulation by Lee (1986) was modified. A flow path was added to represent the flow through the connected joints. The equations for flow are described in Appendix C. Flow through continuous joints reduces h_w/H at the entrance point and increases h_w/H at the exit point and the mean is close to zero. Hence flow through fractures contributes only to the variance of h_w/H. Calculations with the probability distributions of joint dimensions and of K_f were made to obtain the variance of h_w/H given in Table 3c.

2.4. SLOPE STABILITY MODEL

The infinite slope model (Taylor, 1948) has been found to give satisfactory results when there are no abrupt changes in slope and when the failure surface extends only to shallow depths. The safety factor for an infinite slope is

$$F = \frac{c_r + c' + [\gamma H(1 - h_w / H) + (\gamma - \gamma_w) h_w] \tan \varphi'}{\sin \alpha [\gamma H(1 - h_w / H) + \gamma_w h_w]} \qquad [12]$$

where γ and γ_W = unit weights of soil and water, respectively, and h_W = water level in the slope.

The average of H, c' and ϕ' over a pixel (Table 1b, Col.5) are used to calculate the safety factor for the pixel because the pixel is about the size of a small debris flow. The mean and variance of the pixel average are given in Table 1b. The hazard is the failure probability,

$$P_f = P[F_s \leq 1] \qquad [13]$$

The mean and variance of F_S are evaluated by the FOSM from the means and variances of H, c', ϕ' (Table 1b, Cols.5 and 6) and of h_W (Table 3d, Col.5) . P_f is evaluated for each pixel assuming a log-normal distribution for F_S (Ang and Tang,1984).

2.5. MAPPING

Mapping of landslide hazard can be done at different scales and with various degrees of refinement. In this project, mapping was done at two different levels: a macro-map made with regional site conditions and simplified groundwater profile, and a micro map made with local site conditions and a groundwater profile that accounts for catchment shape.

The macro-map shows the hazard over a large area (several km^2), which consists of valley slopes of second- or third-order streams. Reddi's lumped-parameter model was used to calculate h_0 for a plane slope and the average h_w for a slope was taken to be 0.5 h_0 . Regional site conditions (Table 1, col. 2,3, and 4) were used in the calculations.

Micro-maps of landslide hazard were constructed using the following steps: (1) The digital elevation model (DEM) of the U.S. Geological Survey is read into the geographic information system (GIS). MicroImage's Map and Image Processing System (MIPS) and the Spatial Manipulating Language (SML) are used to identify the catchment boundaries and extract the

catchment features, which include the convergence angle β , length L, width B, and slope angle (Fig.5). Specific software used in this project are described in Benosky and Merry (1995). (2) The soil data for each catchment are read into the GIS. (3) The means and variances of the soil properties (Table 1a) are used to calculate the mean and variance of h_0/H . The values of h_w/H at different points within a catchment are obtained using Fig.C.2. (4) The failure probability for each pixel (30x 30m) is computed.

Macro-maps of landslide hazard for Glenoma and Mineral Quadrangles are shown in Figs. 7 and 8. Catchment boundaries and stream lines for Glenoma and Mineral Quadrangles as determined by MIPS and SML are shown in Figs. 9 and 10. The groundwater maps for a 10-year storm for Glenoma and Mineral Quadrangles are shown in Fig. 11 and 12. The micro-maps of landslide hazard for Glenoma and Mineral Quadrangles are shown in Fig. 13 and 14. The narrow white lines on these maps denote streams. Micro-maps made at a scale of 1:24,000 scale are available separately.

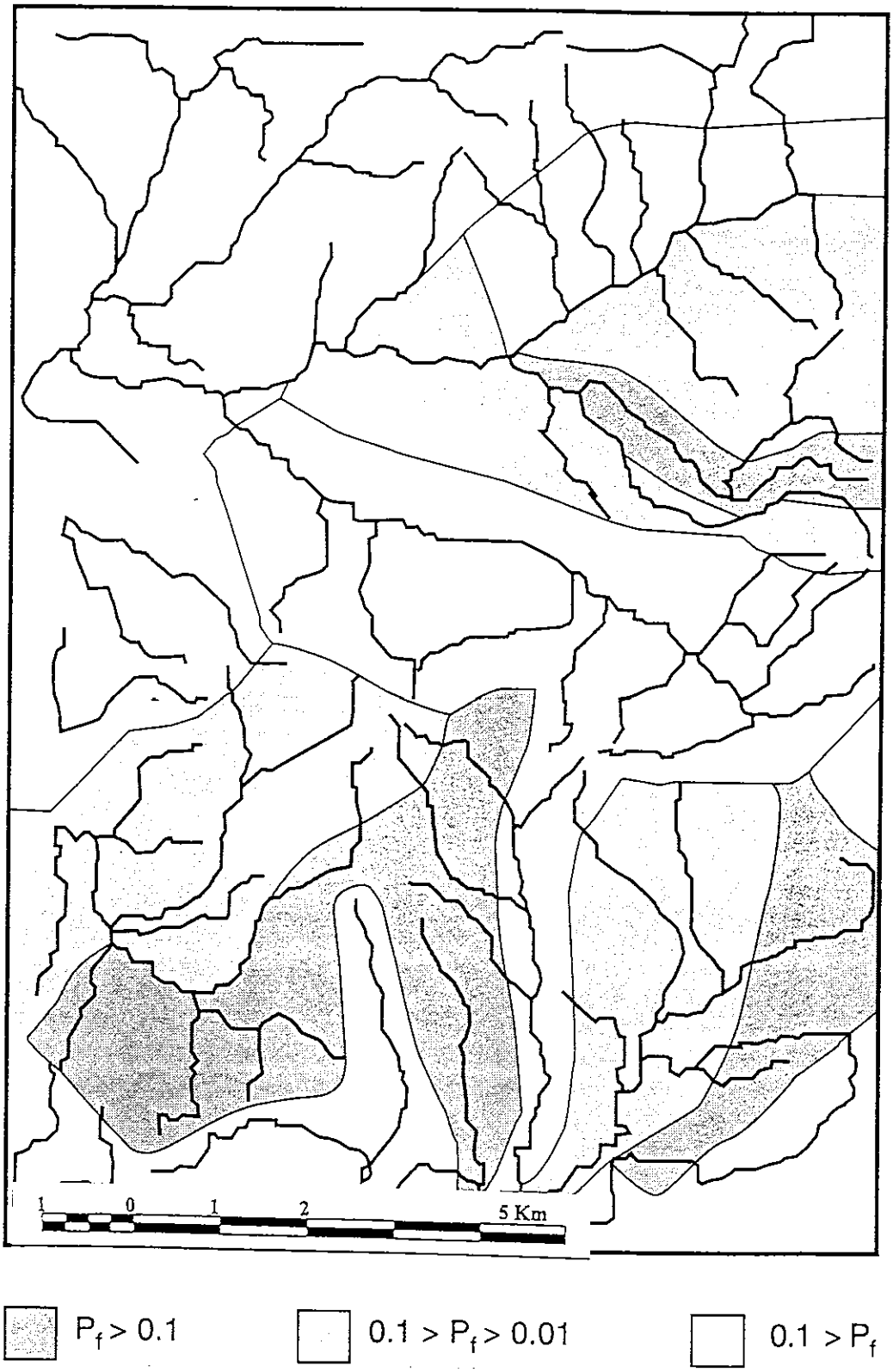

Fig. 7. Macro-map of landslide hazard, Glenoma Quadrangle

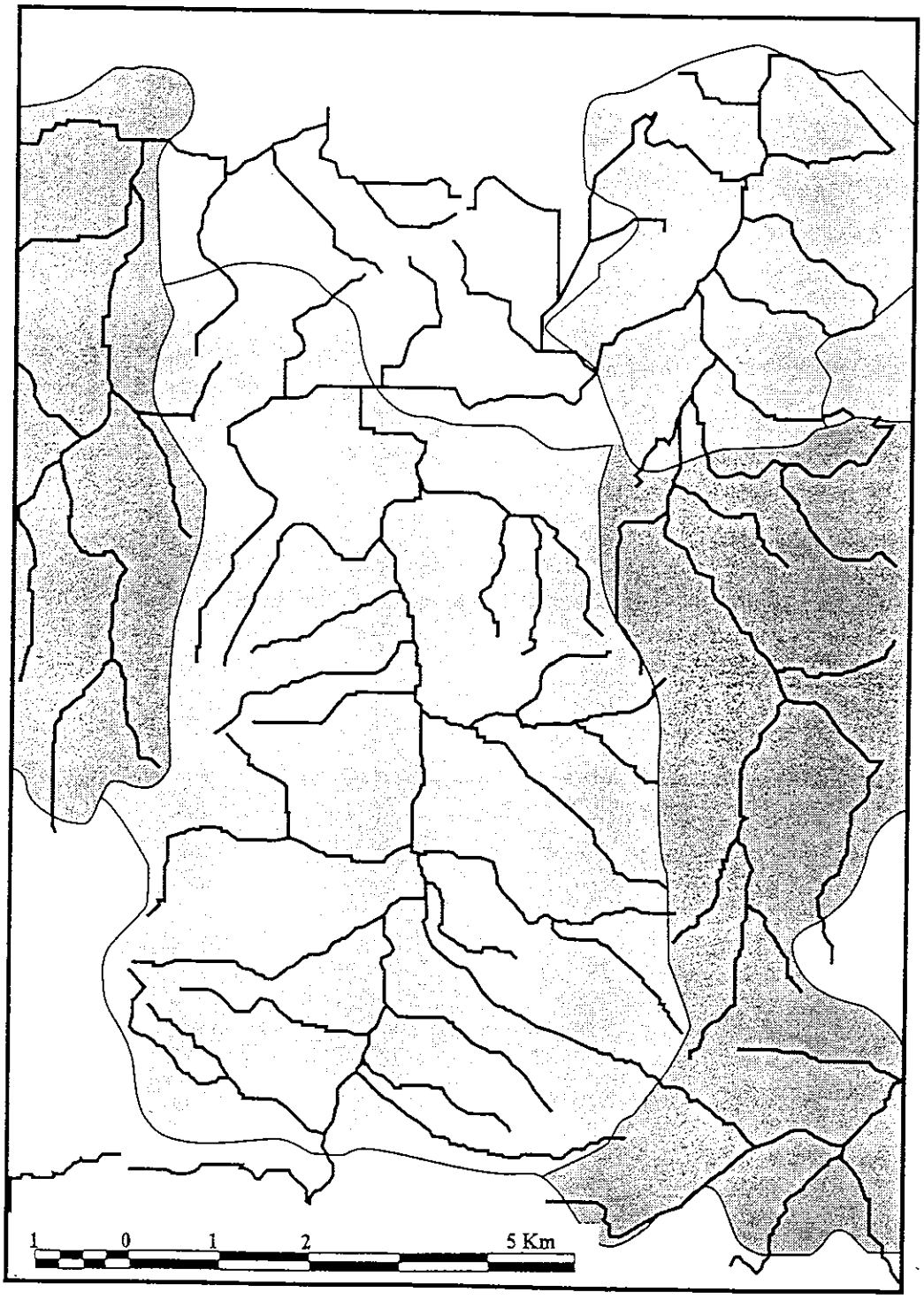

Fig. 8. Macro-map of landslide hazard, Mineral Quadrangle

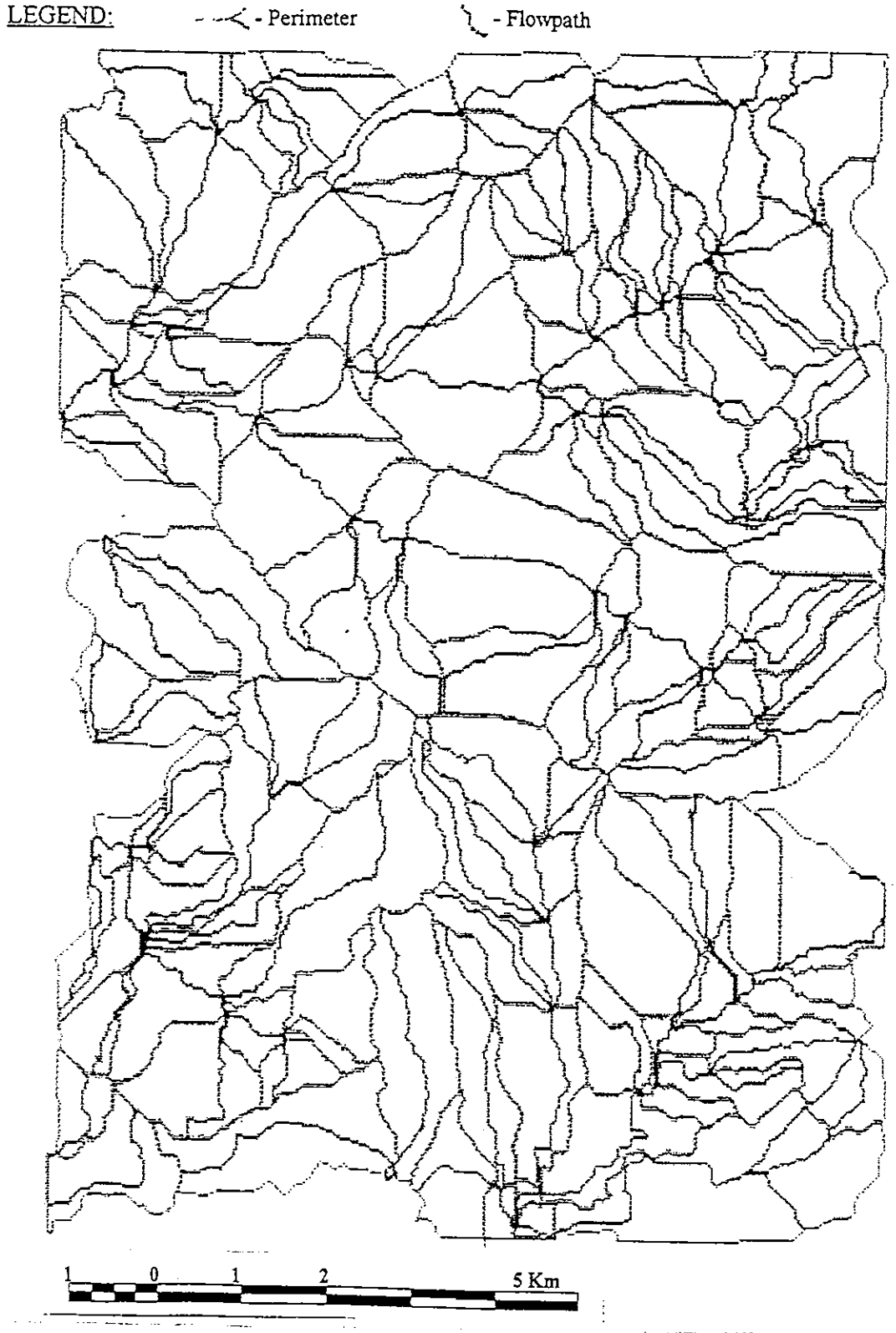

Fig. 9. Flowpath and catchment boundaries, Glenoma Quadrangle

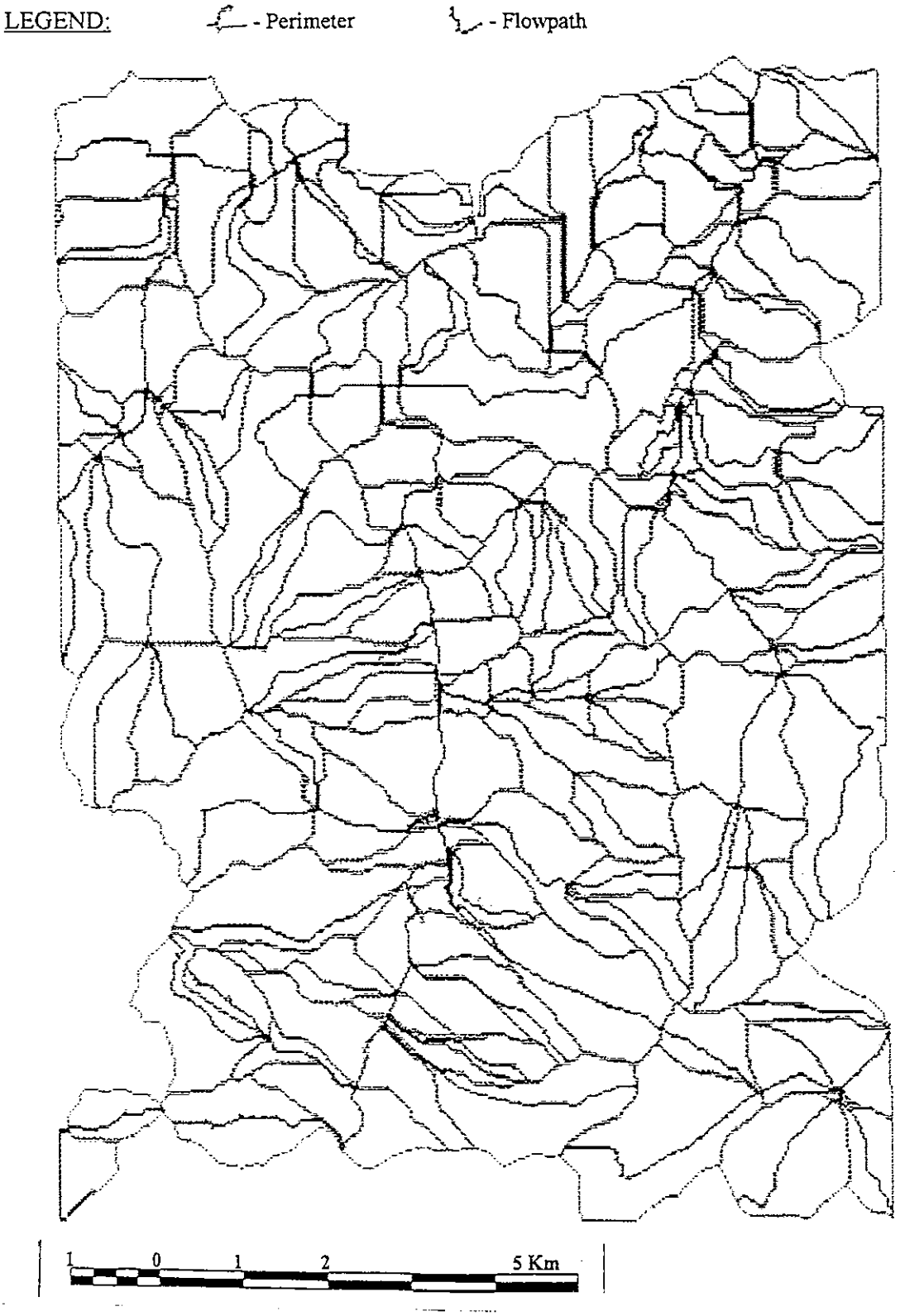

Fig. 10. Flowpath and catchment boundaries, Mineral Quadrangle

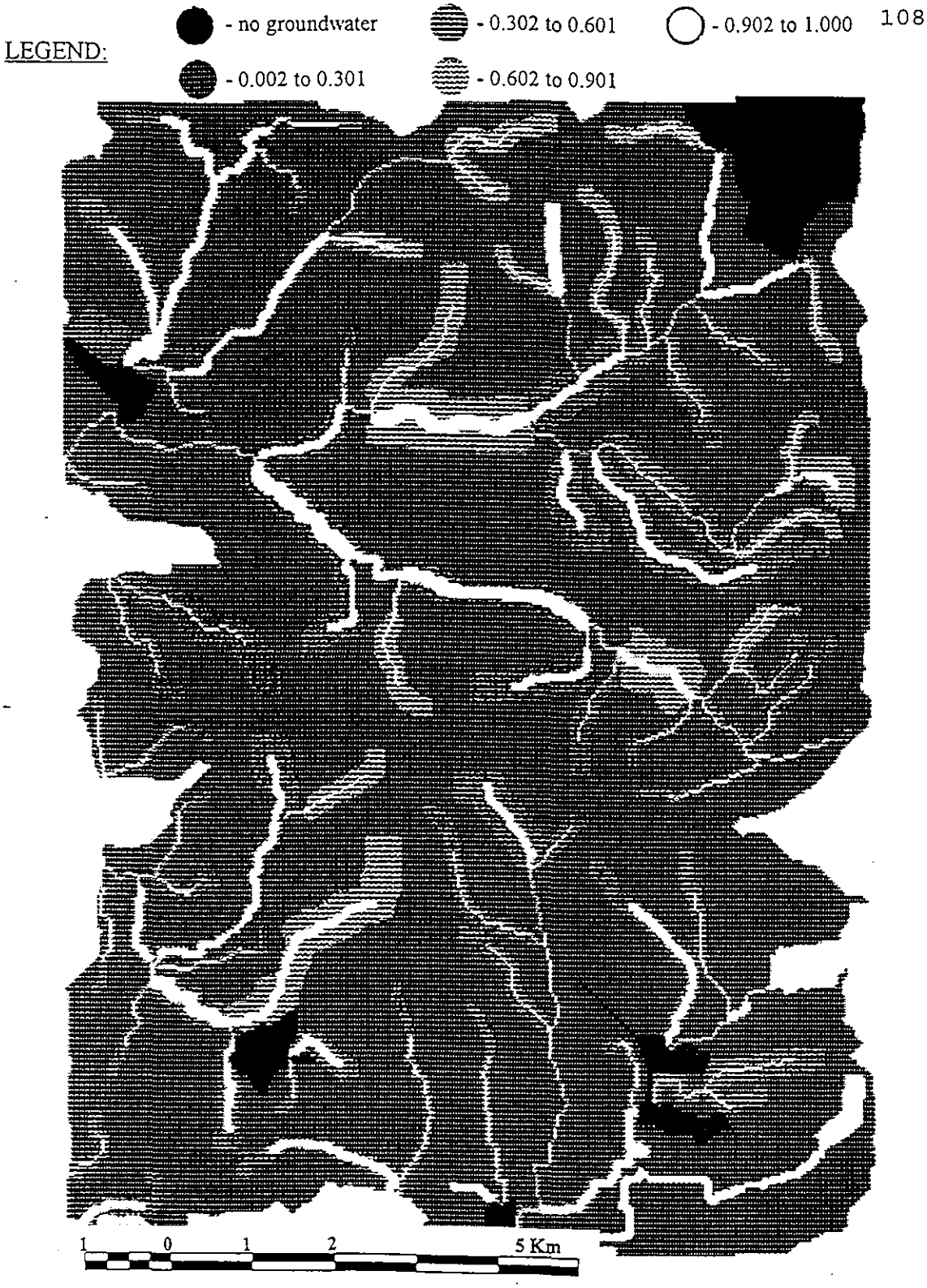

Fig. 11. Groundwater levels (h_w/H) for Glenoma Quadrangle, 10-yr storm

Fig. 12. Groundwater levels (h_w/H) for Mineral Quadrangle, 10-yr storm

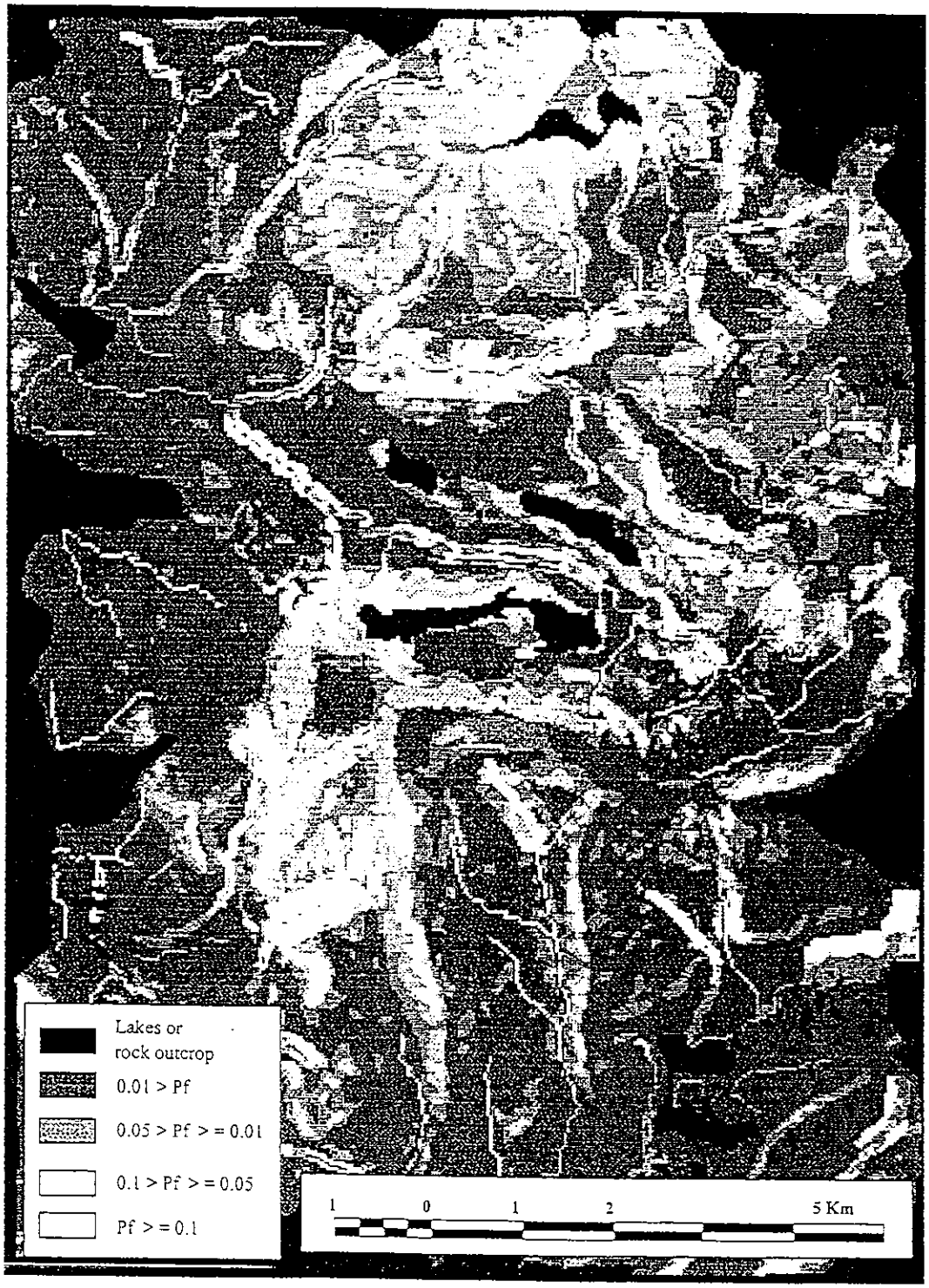

Fig. 13. Micro-map of landslide hazard, Glenoma Quadrangle, 10-yr storm

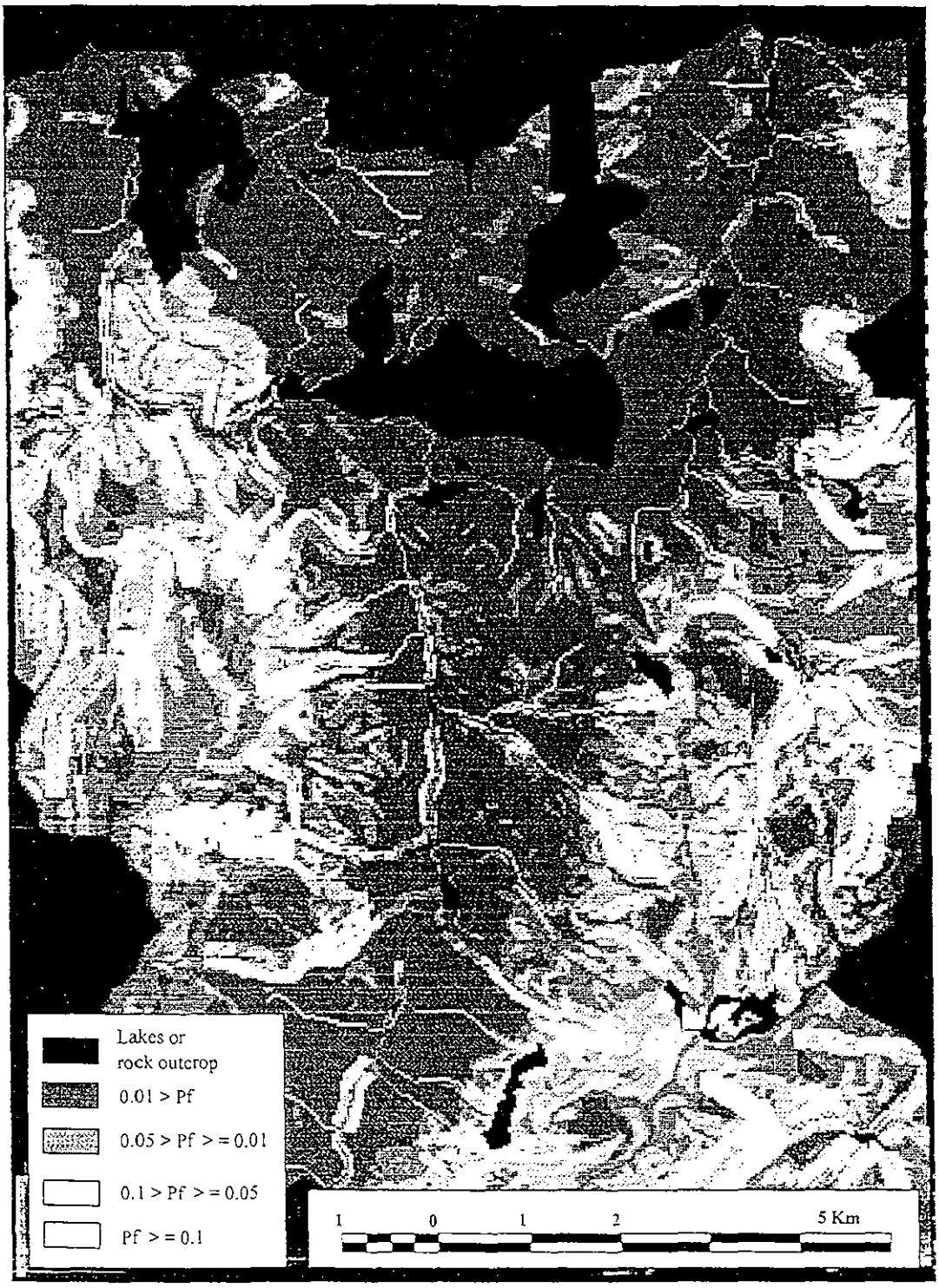

Fig. 14. Micro-map of landslide hazard, Mineral Quadrangle, 10-yr storm

3. SUMMARY AND CONCLUSIONS

A mechanics-based method for landslide hazard prediction is presented. The method incorporates models for rainfall and snowmelt, infiltration into the ground and drainage by gravity flow, and slope stability. The input to the models are storm characteristics, topography and vegetation, geology, and soil properties. Each parameter in the input is expressed in terms of a mean and a variance, which are used to represent the best estimate and the uncertainty, respectively. This allows us to account for different levels of accuracy in the available information and judgment based on field observations. Probability analysis is used to translate the uncertainties into failure probability, which is equal to the landslide hazard.

The method allows mapping of landslide hazard at different scales and with various degrees of refinement. In this project, mapping was done at two different levels: a macro-map made with regional site conditions and simplified groundwater profile, and a micro map made with local site conditions and a groundwater profile that accounts for catchment shape. Macro- and micro-hazard maps were produced for Glenoma and Mineral quadrangles. The cost of producing such maps are relatively low, when compared with the cost of field investigations. Such maps can be used by land managers for preliminary estimates of landslide hazard, and for identifying regions of high hazard that justify more detailed investigations.

The method can also be used to produce more detailed hazard maps for individual catchments where more detailed information is available. The models can readily be adapted to operate on PC's with a compiler. This would make the method useful in offices where large computers are not available.

APPENDIX A. PROBABILITY DISTRIBUTION OF MAXIMUM INFILTRATION

We nee to find the mean and variance of the maximum infiltration, I_n, during the design life of a slope. The pdf of infiltration I during a long continuous storm is given in Eq. [2]. The largest infiltration among n storms is

$$Y_n = \max [X_1, X_2, ...X_n] \qquad [A.1]$$

where X_i = infiltration in a storm. Using the statistics of extremes (eg. Ang and Tang, 1984), the probability density function of Y_n is

$$f_{Yn} = a\, n \exp -n[1 - \exp\{-\exp(ay_n - au)\}] \qquad [A.2]$$

where a and u are the parameters of the extreme value distribution for infiltration. Numerical integration was used to obtain the mean and variance of the maximum infiltration for various n. It is assumed that the number of long continuous storms per year is equal to the average of 2. rom Wu et al (1995) found that, for the storm statistics given in Brunengo (1989), the mean and variance of I are 16 cm and 53/cm^2, respectively. For a design period of 10 yrs, the mean and varaince of I_{10} are derived from the pdf given by Eq [A.2]. The results are given in Table 3a.

APPENDIX B. EFFECT OF ANTECEDENT MOISTURE

Sequence of Storms. The number of storms and the interval between storms affect the antecedent moisture, θ^0 and the initial groundwater level, h_0^0. Brunengo (1989) gave a probability mass function for number of long continuous storms (LCS) per season. The season was defined as Sept.1-June 1. The mean is 2 storms per season. Brunengo (1989) also gave a probability density function for the date of occurrence of a storm Table 1.

For a season with 2 storms, the dates of occurrence, X and Y have the joint distribution

$$f_{X,Y}(x,y) = - \exp[\{-(x-\mu)^2-(y-\mu)^2\}/2\ ^2]/2\ \ ^2 \qquad [B.1]$$

The time interval between storms V = Y - X, has the cumulative distribution function

$$F_V = \int\int f_{X,Y}(x,y)\, dx\, dy\,, \quad X < Y \qquad [B.2]$$

Similar expressions were derived for a season with three storms, with W = Z - Y, where Z is the date of the third storm and W = time interval between the second and third storms.

Small rain events, not classified as LCS, also contribute to antecedent moisture. Table B.1 gives the frequency of small events. The occurrence of small events was assumed to be independent of the LCS. The statistics in Table B.1 were used to determine the average rainfall and average number of small rain events.

Table B.1 Frequency of Small Rain Events (Brunengo, 1989)

Rainfall (cm)	0.25-1.25	1.25-2.50	>2.50
No. of days per year with rainfall	84	41	29

To evaluate the effect of sequence of storms, LCS were assumed to occur at intervals equal to the mean values of V or W. An average number of small rain events, with average rainfall, were assumed to occur during the intervals between LCS. Calculations were made with the lumped-parameter model and properties for 1, 2, .. storms. The antecedent moisture θ_n^0,and initial h_{0n}^0, for the n th storm were taken as the values of θ and h_0 at the mean of V or W after the preceeding storm (Fig.B.1). The values of θ_n^0 and h_{0n}^0 obtained for the different numbers of storms are shown in Fig. B.2, with P (N=n), where N = the number of storms. For each N, θ_n^0 and h_{0n}^0 have conditional distributions $f(\theta_n^0,N)$ and $f(h_0^0,N)$, respectively. The probability density functions of θ_n^0 and h_0^0 are

$$f(\theta) = \Sigma f_\theta(\theta^0|N=n)\, P(N=n) \qquad [B.5a]$$

$$f(h_0^0) = \Sigma f\,(h_0^0|N=n)\, P(N=n) \qquad [B.5b]$$

The distributions $f(\theta^0 N=n)$ and $f(h_0^0 N=n)$ may be calculated with the mean and variance of W and Z. However, Abdel-Latif(1994) has shown that the effect of W or Z on the variance of ^{0} and h_0^0 are minor. Hence, simplified calculations assuming that $\theta^0|N=n$ and $h_0^0|N=n$ are discrete and equal to their mean values provide a satisfactory estimate of the mean and variance of θ^0 and h_0^0. Then,

$$p(\theta^0) = \theta_n^0\, P(N=n) \qquad [B.6]$$

The same procedure was used to calculate $p(h_0^0)$ and the distributions of θ^0 and h_0^0 were used to calculate the variance of h_0 due to number of storms, which is listed in Table 2a.

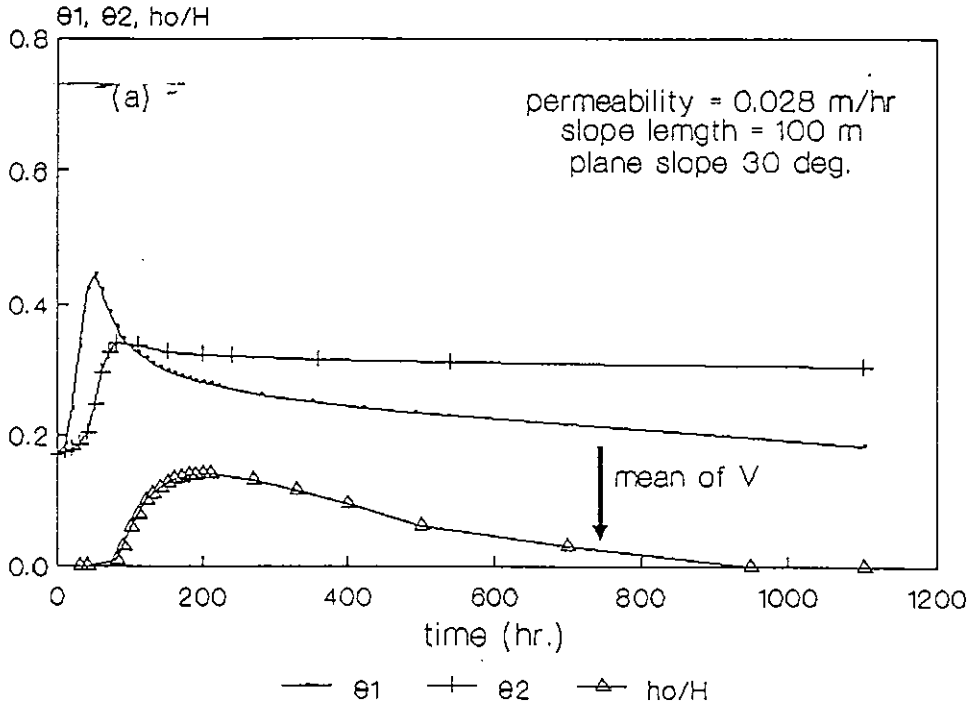

Fig. B1. Antecedent Moisture as a function of time

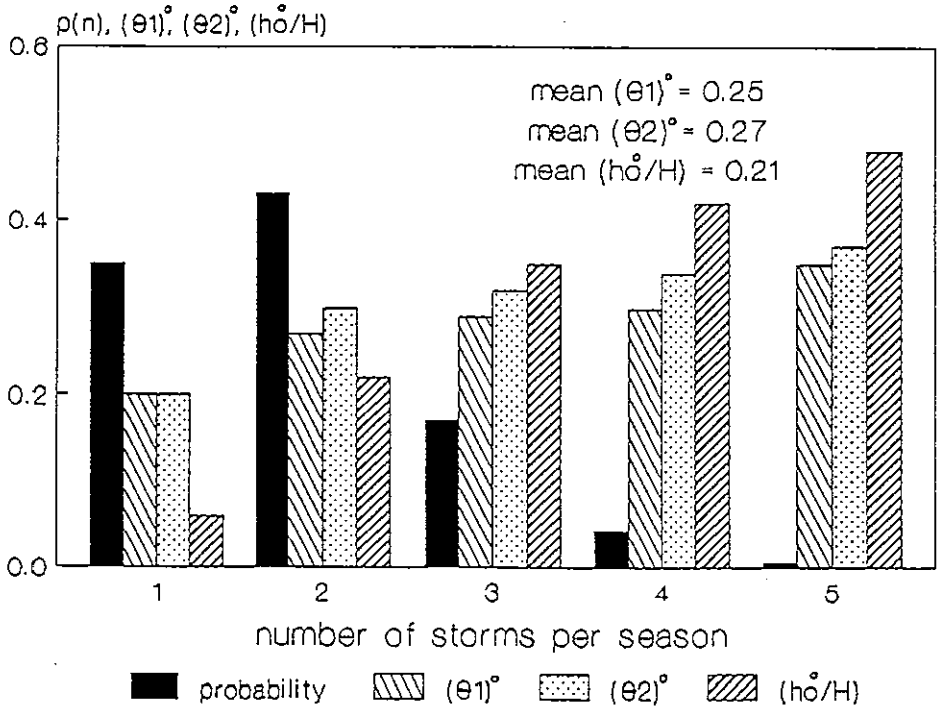

Fig. B2. Probability mass function, p(n), of number of storms per season, and antecedent moisture as a function of number of storms per season

APPENDIX C. FINITE DIFFERENCE SOLUTION

WATER LEVEL AT A POINT. For the finite difference solution, we adopt the extended Dupuis-Forchheimer assumption; that is, the streamlines are parallel to the X-axis, Fig. C.1. The continuity equation is (Lee,1986)

$$C\frac{\partial h_w}{\partial t}=Q_r\cos\alpha+\frac{\partial}{\partial y}[K_s h_w(\cos\alpha(\frac{\partial h_w}{\partial y}+\frac{\partial H_t}{\partial y}-\frac{\partial H}{\partial y})+\tan\gamma)]+\frac{\partial}{\partial x}[K_s h_w(\cos\alpha(\frac{\partial h_w}{\partial x}+\frac{\partial H_t}{\partial x}-\frac{\partial H}{\partial x})+\sin\alpha)] \qquad [C1]$$

where H, H_t = dimensions as shown in Fig. C.1a.

We need to estimate the water level h_w at different points within the catchment shown in Fig. 5b. Values of h_W were calculated for catchments, which were represented as concave slopes with different α's, β 's and L's (Fig.5). The surface of the catchment is represented as a part of a cone, shown as aba'c in Fig. C.2.

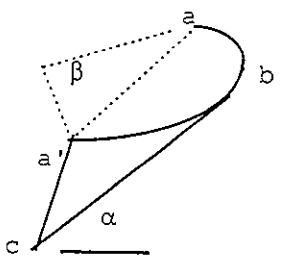

Fig. C.2. Conical surface of catchment.

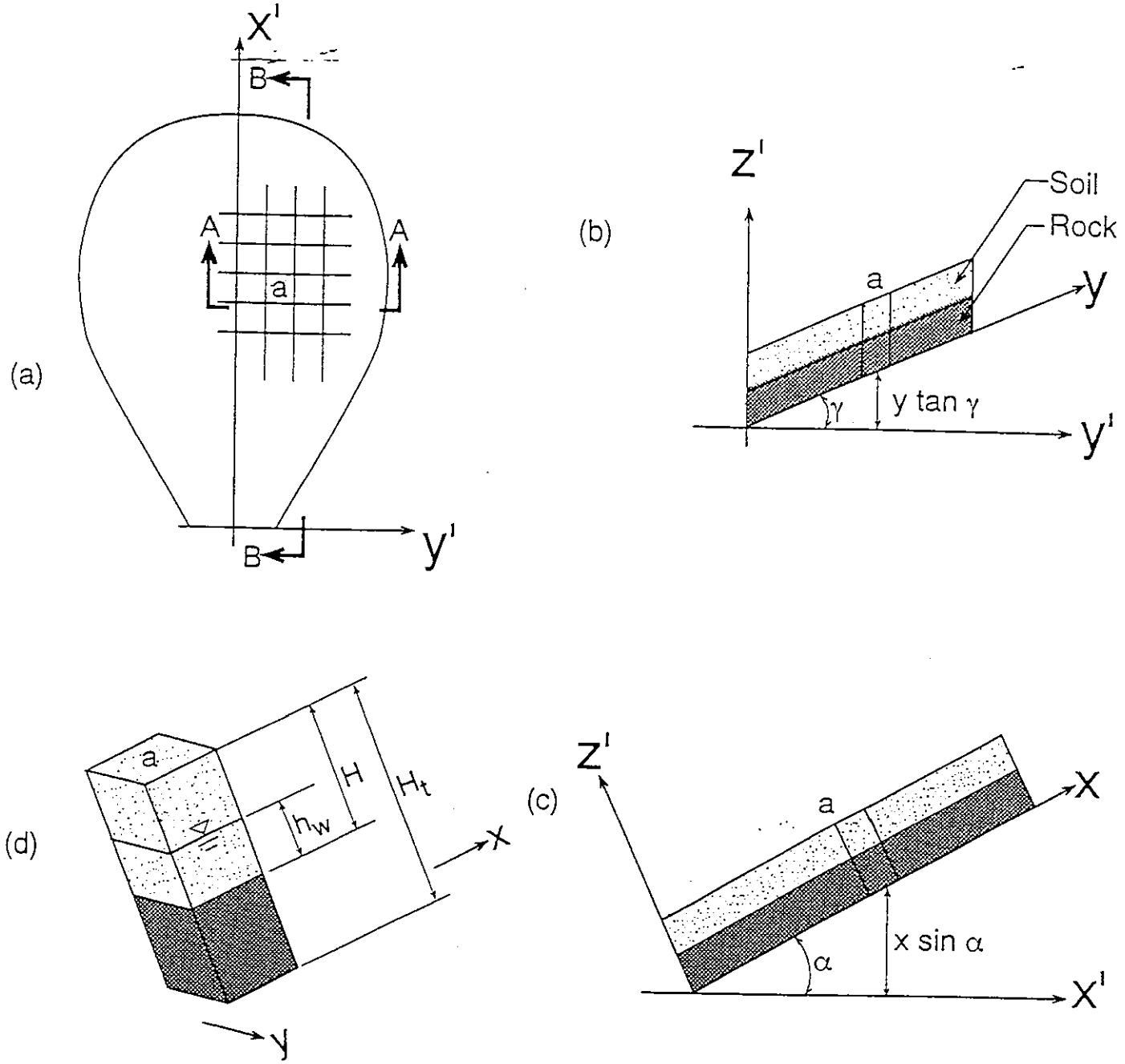

Fig. C.1. Finite Difference Model.

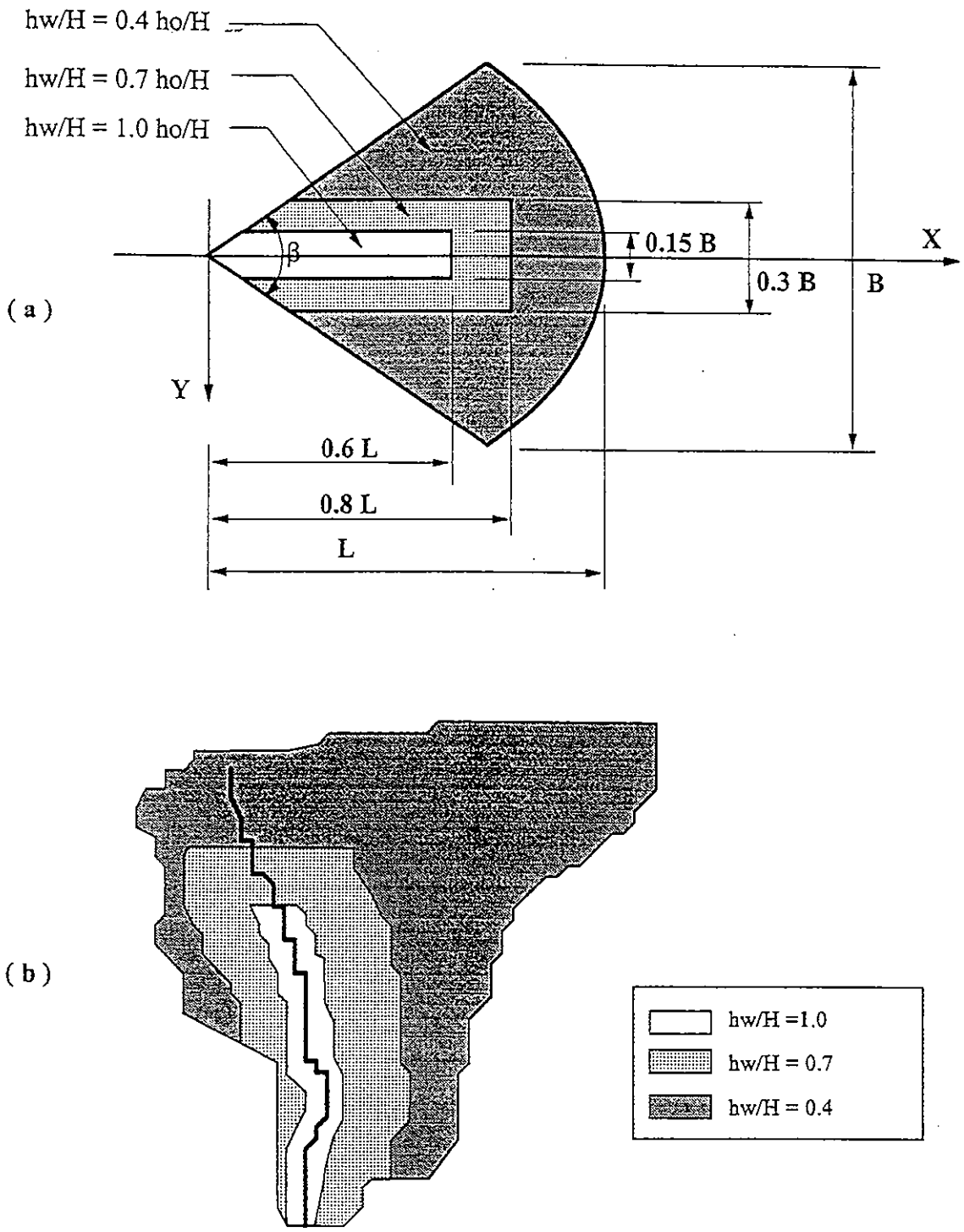

Fig. C3. Simplified distribution of h_w (a) Simplified catchment, (b) Catchment 77.

The results from such calculations are used to construct the simplified distribution of h_W shown in Fig. C3a, where h_W is shown as a fraction of h_0. Fig. C.3a is used to estimate h_W at various points in a catchment. give h_w/H. An example of the values of h_w/H calculated for Catchment 77 is shown in Fig. C.3b.

FLOW THROUGH FRACTURES. The irregular flow path through the fractures is represented by a circular arc, Fig. C4. This has little effect on the results because the head difference between points 1 and 2 depends primarily on the length of the flow path. The continuity equation for this condition is

$$C\frac{\partial h_w}{\partial t}=Q_r\cos\alpha-Q_f+\frac{\partial}{\partial y}[K_s h_w(\cos\alpha(\frac{\partial h_w}{\partial y}+\frac{\partial H_t}{\partial y}-\frac{\partial H}{\partial y})+\tan\gamma)]+\frac{\partial}{\partial x}[K_s h_w(\cos\alpha(\frac{\partial h_w}{\partial x}+\frac{\partial H_t}{\partial x}-\frac{\partial H}{\partial x})+\sin\alpha)] \qquad [C2]$$

at node 1 and

$$C\frac{\partial h_w}{\partial t}=Q_r\cos\alpha+Q_f+\frac{\partial}{\partial y}[K_s h_w(\cos\alpha(\frac{\partial h_w}{\partial y}+\frac{\partial H_t}{\partial y}-\frac{\partial H}{\partial y})+\tan\gamma)]+\frac{\partial}{\partial x}[K_s h_w(\cos\alpha(\frac{\partial h_w}{\partial x}+\frac{\partial H_t}{\partial x}-\frac{\partial H}{\partial x})+\sin\alpha)] \qquad [C3]$$

at node 2, where C = specific yield, Q_r = recharge to the saturated zone, and

$Q_f = i_f\ K_f$ [C4]

$i_f = 2\ \{x + (h_{w,1}-h_{w,2})\cos\alpha\}/\pi\ a_f$ [C5]

where x = difference in elevation between points 1 and 2, b_f = width of fracture, a_f = distance between entrance and exit, K_f = transmissibility of fracture, Q_f = flow through fracture, t = time, h_{W1}, h_{W2} = heads at nodes 1 and 2.

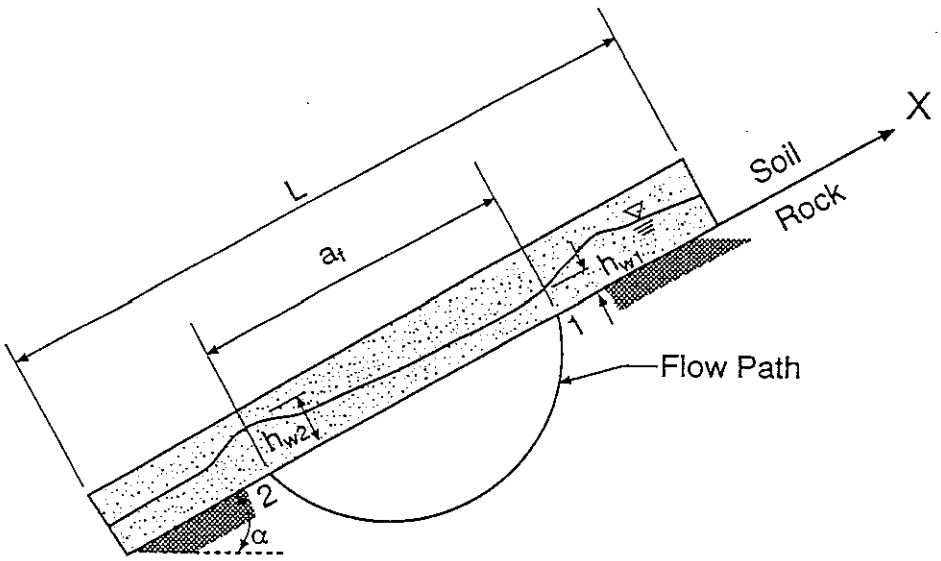

Fig. C4. Flow through fractures in bedrock.

APPENDIX D. REFERENCES

Abdel-Latif, M. A. (1994) Assessment of landslide hazard. Ph.D. dissertation, Ohio State Univ., Columbus.

Ang, A. H-S., and Tang, W.H. (1975) *Probability Concepts in Engineering Planning and Design*, Vol.1, John Wiley and Sons, New York, 409p.

Ang, A. H-S., and Tang, W.H. (1984). *Probability Concepts in Engineering Planning and Design, Vol.2*, John Wiley and Sons, New York, 562p.

Benosky, C.P., and Merry, C.J. (1995) Automatic extraction of watershed characteristics using spatial analysis techniques with application to groundwater mapping. Journal of Hydrology, in press.

Berris, S.N., and Harr, R.D. (1987) Comparative snow accumulation and melt during rainfall in forests and clear-cut plots in the western Cascades of Oregon. Water Resources Research, 23 (1): 135-141.

Beven, K. (1981) Kinematic subsurface stormflow. Water Resources Research, 17:1419-1424.

Beven, K. (1982) On subsurface stormflow: predictions with simple kinematic theory for saturated and unsaturated flows. Water Resources Research, 18:1627-1633.

Beven, K., and Germann, P. (1982) Macropores and water flow in soils. Water Resources Research, 18 (5):1311-1325.

Brabb, E.E., Pampeyan, E.H., and Bonilla, M.G.(1972) Landslide susceptibility in San Mateo County, California. U.S. Geological Survey Miscellaneous Field Studies Map MF-360.

Bras, R.L., and Rodriguez-Iturbe, I. (1985) *Random Functions and Hydrology*. Addison-Wesley Pub. Co., 559p.

Brunengo, M.J. (1989) Frequency characteristics of winter storm precipitation in the central Washington Cascades. Unpublished report, Washington Dept. of Natural Reources, Olympia.

Buchanan, P., Savigny, K.W., and de Vries, J.(1990) A model of modeling water tables at debris avalanche headscarps. Journal of Hydrology, 113:61-88.

Campbell, G.S. (1974) A simple method for determining unsaturated conductivity from moisture retention data. Soil Science, 117:311-314.

Carrara, A., Cardinali, R., Detti,F., Guzzett, V., Pasqui, V., and Reichenbach, P. (1991) GIS techniques and statistical models in evaluating landslide hazard. Earth Surface Processes and Landforms, 16:, 427-445.

Clapp, R.B., and Hornberger, G.M. (1978) Empirical equations for some soil hydraulic properties. Water Resources Research, 14 (4):601-604.

Eagleson, P.S. (1978) Climate, soil, vegetation, Parts 3 and 4. Water Resources Research, 14:731-739, 741-748.

Einstein, H. (1988) Landslide risk assessment procedure. Fifth International Symposium on Landslides, Lausanne, 2:1075-1090.

Fell, R. (1991) A model for prediction of piezometric levels in landslides. In Slope Engineering, Thomas Telford, London, 37-42.

Freeze, R.A. (1971) Three-dimensional, transient, saturated-unsaturated flow in a groundwater basin. Water Resources Research, 7: 347-366.

Hammond, C., Hall, D., Miller, S., and Swetik, P.(1992) Level 1 stability analysis (LISA). General Technical Report INT-285, Forest Service, U.S.Dept. of Agriculture.

Hoek, E., and Bray, J.W. (1981) Rock Slope Engineering. Institution of Mining and Metallurgy, London.

Huitt, J.L., (1956) Fluid flow in simulated fracture. Journal American Institute of Chemical Engineering, 2:259-264.

Lee, I-M. (1986) A probabilistic analysis of pore water predictions for unsteady groundwater flow on a sloping bed. Ph. D. dissertation, Ohio State University.

Louis, C. (1969) A study of groundwater flow in jointed rock and its influence on the stability of rock masses. Doctoral Thesis, Univ. of Karlsruhe (in German), Rock Mechanics Research Report No.10, Imperial College (English translation), 90p.

Lumb, P. (1975) Spatial variability of soil properties. Proc. 2nd International Conference on Application of Statistics and Probability in Soil and Structural Engineering, Aachen, 2:397-421.

O'Loughlin,E.M. (1986) Prediction of surface saturation zones in natural catchments by topographic analysis. Water Resources Research, 22:794-804.

Reddi, L.N., and Wu. T.H. (1991) Probability analysis of groundwater levels in hillside slopes. J. Geotechnical Engineering, ASCE, 117 (6):872-890.

Richards, L.A. (1931) Capillary conduction of liquids through porous mediums, Physics 1:318-333.

Sammori, T, and Tsuboyama (1991) Parametric study on slope stability with numerical simulation in consideration of seepage process. In *Landslides*, D.H.Bell, ed., Balkema, Rotterdam,

Schroeder, W.L. (1983) Geotechnical properties of southeast Alaskan forest soils. Civil Engineering Dept., Oregon State Univ. Corvallis, 45p.

Sloan, P.G., and Moore, I.D.(1984) Modeling subsurface storm-flow on steeply sloping forested watersheds. Water Resources Research, 20(12): 1815-1822.

Soil Conservation Service (1987) Soil survey of Lewis County area, Washington. U.S. Dept. of Agriculture.

Tang, W.H. (1984) Principles of probabilistic characterization of soil properties. ASCE, New York 74-89

Tang, W.H., and Gilbert, R.B.(1988) Statistics of spatial average in a random two-state medium. Structural Safety, 6:271-282.

Taylor, D.W. (1948) *Fundamentals of Soil Mechanics*, John Wiley and Sons, New York.

Terzaghi, K. (1950) Mechanism of landslides. Engineering Geology Volume, Geological Soc. America, 83-123.

Vanmarcke, E.H. (1977) Probabilistic modeling of soil profiles. J. Geotechnical Engineering Div., ASCE,103:1227-1246.

Wagner, A., Olivier, R., and Leite, E.(1987) Rock and debris slide risk maps applied to low-volume roads in Nepal. Transportation Research Record, 1106:255-267.

Ward, T.J., Li, R-M., and Simons, D.B. (1978) Landslide potential and probability considering randomness of controlling factors. 1st International Conference on Reliability in Water Resources, Ottawa, 592-608.

Wieczorek, G. (1984) Preparing a detailed landslide-inventory map for hazard evaluation and prediction. Bulletin of Assoc. of Engineering Geologists, 21:337-342.

Wu, T.H. (1989) Variability of geologic materials. In *The Art and Science of Geotechnical Engineering*, ed. E.J. Cording, W.J. Hall, J.D. Haltiwanger, A.L. Hendron, and G. Mesri. Prentice Hall, Englewood, NJ, 221-239.

Wu, T.H., Abdel-Latif, Wiberg, E., and Brunengo, M.J.(1995) Probability distribution of rain-plus-snowmelt in Washington Cascades. Proc. 7th Intern. Conf. on Applications of Statistics and Probability, 1:565-571.

Wu, T.H., Merry, C.J., Abdel-Latif, M., and Benosky, C.P. (1993) Landslide Hazard Mapping, 1. Estimsating Piezometric Levels. Report to CMER Comm., Washington Timber/Fish/Wildlife Agreement. Civil Engineering Dept., Ohio State Univ., Columbus.

Wu, T.H., and Swanston, D.N. (1980) Risk of landslides in shallow soils and its relation to clear-cutting in Southeastern Alaska. Forest Science, 26:495-510.

APPENDIX E. NOTATIONS

a b c = dimensions

B = width of catchment; constant for unsaturated permeability

c'= cohesion in terms of effective stress

c_r = shear strength due to roots

D = duration of rainstorm

f( ) = probability density function

F_s = factor of safety

H = depth of soil layer

h_0 = piezometric height at exit point of catchment

h_w = piezometric height at any point

I = infiltration

K = coefficient of permeability

k = constant in melt equation

L = length of catchment

M = snowmelt

M_p = potential snowmelt

P[ ]= probability

R = rainfall

S = snow-water-equivalent

T = air temperature

t = date of storm

U = wind velocity

α = slope angle

β = convergence angle

γ = unit weight

Δ = coefficient of variation = σ/μ

δ = correlation distance

θ = volumetric moisture content

ψ = potential = negative suction

σ = standard deviation

μ = mean